

A probable inside-out dwarf nova outburst from the period bouncer candidate ASASSN-25dc

Yusuke Tampo,^{1,2*} Naoto Kojiguchi,^{3,4} Mariko Kimura,⁵ Keisuke Isogai,^{3,6} David. A. H. Buckley,^{1,2,7} Nikita Rawat,¹ Stephen B. Potter,^{1,8} Anke van Dyk,^{1,2} Patrick Woudt,² Paul J. Groot,^{1,2,9} Franz-Josef Hambsch,^{10,11,12} Berto Monard,¹³ Peter Starr,¹⁴ William Goltz,¹⁵ Daisaku Nogami,⁴ and Taichi Kato⁴

¹South African Astronomical Observatory, PO Box 9, Observatory, 7935, Cape Town, South Africa

²Department of Astronomy, University of Cape Town, Private Bag X3, Rondebosch 7701, South Africa

³Okayama Observatory, Kyoto University, 3037-5 Honjo, Kamogatacho, Asakuchi, Okayama 719-0232, Japan

⁴Department of Astronomy, Kyoto University, Kitashirakawa-Oiwake-cho, Sakyo-ku, Kyoto 606-8502, Japan

⁵Advanced Research Center for Space Science and Technology, Colledge of Science and Engineering, Kanazawa University, Kakuma, Kanazawa, Ishikawa 920-1192, Japan

⁶Department of Multi-Disciplinary Sciences, Graduate School of Arts and Sciences, The University of Tokyo, 3-8-1 Komaba, Meguro, Tokyo 153-8902, Japan

⁷Department of Physics, University of the Free State, P.O. Box 339, Bloemfontein 9300, South Africa

⁸Department of Physics, University of Johannesburg, PO Box 524, Auckland Park 2006, South Africa

⁹Department of Astrophysics/IMAPP, Radboud University, PO Box 9010, 6500 GL Nijmegen, The Netherlands

¹⁰Groupe Européen d'Observations Stellaires (GEOS), 23 Parc de Levesville, 28300 Bailleau l'Evêque, France

¹¹Bundesdeutsche Arbeitsgemeinschaft für Veränderliche Sterne (BAV), Munsterdamm 90, 12169 Berlin, Germany

¹²Vereniging Voor Sterrenkunde (VVS), Zeeweg 96, 8200 Brugge, Belgium

¹³Kleinkaroo Observatory, Center for Backyard Astrophysics Kleinkaroo, Sint Helena 1B, PO Box 281, Calitzdorp 6660, South Africa

¹⁴Dubbo Observatory, 17L Camp Rd, Dubbo NSW 2830, Australia

¹⁵Association of Variable Star Observers (AAVSO), 185 Alewife Brook Parkway, Suite 410, Cambridge, MA 02138, United States of America

Accepted XXX. Received YYY; in original form ZZZ

ABSTRACT

We report optical time-resolved photometric observations of a newly-discovered outbursting system, ASASSN-25dc. Its 8-mag amplitude, 40-day duration, 1-mag dip in the outburst plateau, and positive superhumps are characteristic of a dwarf nova super-outburst in a non-magnetic cataclysmic variable. We establish its stage-A and stage-B superhump periods as 0.059387(5) d and 0.058864(3) d, respectively. The negative superhump period derivative ($-1.4(2)\times 10^{-5}$ cycle⁻¹) during the stage-B superhumps and the empirical relation indicate the mass ratio is 0.054(7), below the period bounce range. The long outburst decline timescale (35.2(1) d mag⁻¹) and small superhump amplitude (≈ 0.08 mag) observed in ASASSN-25dc are also seen in some period bouncer systems, but not seen in systems well before the period bounce. Despite its short superhump period and indicated small mass ratio, we find no evidence of the excitement of the 2:1 tidal resonance. Moreover, its outburst rise timescale (1.62(9) d mag⁻¹) is significantly longer than those measured at less than 0.4 d mag⁻¹ in other dwarf nova outbursts around the period minimum. Overall, an inside-out dwarf nova outburst from a massive disc in a system with a mass ratio around or even below the period minimum, but lacking the 2:1 tidal resonance, may explain all these observations. However, this challenges the existing models of dwarf nova superoutbursts, which do not predict these outburst properties in low-mass-ratio systems.

Key words: accretion, accretion discs — novae, cataclysmic variables — stars: dwarf novae — stars: individual (ASASSN-25dc)

* E-mail: yusuke@sao.ac.za (YT)

1 INTRODUCTION

Cataclysmic variables (CVs) are close binary systems that host an accreting white dwarf (WD) and a mass-transferring low-mass secondary star that fills its Roche lobe (see Warner 1995; Hellier 2001, for a general review). In a non-magnetic CV, the transferred gas forms an accretion disc around the WD. Because of the mass transfer and the angular momentum loss, CVs evolve towards shorter orbital periods and smaller mass ratios (Robinson 1983; King 1988). Magnetic braking is responsible for the angular momentum loss for a system above the period gap, while gravitational wave radiation is considered to play the role below the period gap. At the point when the secondary mass reaches $0.06\text{--}0.07 M_{\odot}$ (Knigge et al. 2011; McAllister et al. 2019), the secondary becomes degenerate, altering its mass-radius relation. After this point, a CV system evolves towards a longer orbital period, observed as the period minimum around 80 min or 0.056 d (Gänsicke et al. 2009). CVs that have passed through the period minimum are called a period bouncer system.

Dwarf novae (DNe) form a major subtype in non-magnetic CVs. They show repeating outbursts with an amplitude of 1–9 mag, a duration of a few days–a month, and a cycle of weeks to decades in optical. These outbursts are understood in the thermal instability model in an accretion disc (Osaki 1996; Kimura 2020; Hameury 2020). In quiescence, a disc grows its mass with a constant mass transfer rate from the secondary star. Once its surface density reaches a critical value, the disc transitions into its high state with a higher accretion rate, observed as an outburst. All DN outbursts can be divided into two classes with respect to which disc radii the heating wave starts to propagate: inside-out and outside-in outbursts. Because the critical surface density has a $r^{1.05}$ dependence on the disc radius r (Cannizzo et al. 1988), outside-in outbursts are expected to have a shorter rise timescale τ_{rise} to the outburst maximum (Mineshige & Osaki 1985). This has indeed been observed in the case of SS Cyg, which shows a bimodal distribution of the rise timescale (Cannizzo & Mattei 1998).

CVs around the period minimum, typically with a mass ratio q lower than 0.1, form a WZ Sge-type DN subclass (Kato (2015) for a review). Their outbursts are accompanied by two types of short-period modulations known as superhumps: early and ordinary superhumps. These outbursts, accompanied by superhumps, are called superoutbursts. Early superhumps are double-peaked modulations with a superhump period P_{SH} almost equal to the orbital one P_{orb} , which are suggested to originate from the double-arm structure in the disc excited by the 2:1 tidal resonance (Lin & Papaloizou 1979; Osaki & Meyer 2002; Uemura et al. 2012). Ordinary superhumps follow with a superhump period a few percent longer than the orbital period. This is understood as a precession of the eccentric disc deformed by the 3:1 tidal resonance (Whitehurst 1988; Hirose & Osaki 1990). Kato et al. (2009) established three stages of ordinary superhumps (stages A, B, and C) based on the superhump period changes. The superhump period derivative ($P_{\text{dot}} = \dot{P}_{\text{SH}}/P_{\text{SH}}$) is often defined for stage-B ordinary superhumps. Because the 2:1 resonance suppresses the growth of the 3:1 resonance (Lubow 1991a), early superhumps are always observed before ordinary superhumps. It has been found that some outbursts in WZ Sge-type DNe lack apparent early superhumps due to (A) a low inclination, although the 2:1 resonance is excited and a faster powerlaw outburst decline corresponding to the early superhump phase is observed (e.g., GW Lib; Cannizzo 2001; Kato et al. 2009), and (B) a less energetic outburst, where a disc does not reach the 2:1 resonance radius and the 2:1 resonance is not excited (e.g., the 2015 outburst of AL Com; Kimura et al. 2016).

The behaviour of superhumps strongly depends on the mass ratio of

the system. Indeed, several methods have been proposed to estimate the binary parameters from superhumps (e.g., Patterson et al. 2005; Kato & Osaki 2013b). Nakata et al. (2014); Kimura et al. (2018) suggested some smoking-gun features for a DN outburst in a system with a mass ratio below the period minimum; (1) multiple rebrightening outbursts or a dip in brightness during the superoutburst plateau (double superoutburst), (2) long duration (≥ 100 cycles) of stage-A superhump phase, (3) large period decrease ($\geq 2\%$) between the stage-A and stage-B superhumps, (4) small superhump amplitude (≤ 0.1 mag), (5) long delay (≥ 10 d) of ordinary superhump emergence, (6) a long outburst decline timescale (≥ 20 d mag $^{-1}$) in the ordinary superhump phase, and (7) large outburst amplitude at the time of appearance of ordinary superhumps. We note that, as discussed in the above papers, not all period bouncers necessarily show all these features.

Some aspects of the outburst mechanism in WZ Sge-type DNe remain unclear (e.g., see discussion in Kato 2015; Hameury 2020), especially on how their outbursts are triggered. Both the thermal-tidal instability and enhanced mass transfer models predict that superoutbursts in a system around the period minimum are always triggered as an outside-in outburst to account for the observed outburst energetics and cycles (Osaki 1995; Lasota et al. 1995; Hameury et al. 1997; Meyer-Hofmeister et al. 1998). The only observational evidence is their short rise timescales (≈ 0.2 d mag $^{-1}$) observed in several samples with limited cadence (Patterson et al. 1981; Maehara et al. 2009; Vican et al. 2011), and recently confirmed with TESS observations (Tampo et al. 2026).

ASAS-SN reported the discovery of ASASSN-25dc on 2025 July 13.1 UTC (BJD 2460869.6) at $g = 13.07$ mag. Both ASASSN and ATLAS detected the outburst rise since BJD 2460860.5, which attributes a slow rise to the outburst maximum for a week. The quiescence counterpart is the Gaia object 6129070308813533568 of $G = 21.00(2)$ mag (Gaia Collaboration et al. 2021). Hence, the outburst amplitude is ≈ 8.0 mag. There is no available parallax in Gaia. Ordinary superhumps were detected, and their preliminary period was determined as 0.05991(4) d, suggesting its classification as a WZ Sge-type DN (vsnet-alert 28089¹). This paper is structured as follows: Section 2 summarises an overview of our observations and analysis. Section 3 presents the result of the overall superoutburst and superhumps of ASASSN-25dc. In section 4, we discuss our identification of ASASSN-25dc as an inside-out outburst in a period bouncer system, and further implications on the disc instability model. Section 5 summarises the paper. All observation epochs in this paper are described in the Barycentric Julian Day (BJD).

2 OBSERVATIONS AND ANALYSIS

2.1 Ground-based time-resolved observations

Our ground-based time-resolved photometric observations of ASASSN-25dc were carried out through the Variable Star Network (VSNET) collaboration (Kato et al. 2004). We also obtained the time-series observations using the Mookodi (Erasmus et al. 2024) on the Lesedi telescope and the SHOC (Cophejans et al. 2013) on the 1.0-m telescope, both located at the Sutherland Observatory of the South African Astronomical Observatory. Their instrument details and observation logs are summarised in tables A2 and A3, respectively. The zero point of the observations with the clear band was adjusted

¹ <http://ooruri.kusastro.kyoto-u.ac.jp/mailarchive/vsnet-alert/28089>

to the V -band magnitude of standard stars (CV band). Before period analysis, the global trend of the outburst decline was removed by subtracting a smoothed light curve obtained by locally weighted polynomial regression (LOWESS; Cleveland 1979). The superhump maxima were determined following Kato et al. (2009); Kato & Osaki (2013a). The phase dispersion minimisation (PDM; Stellingwerf 1978) method was applied for the determination of superhump periods in this paper. The 1σ error for the PDM analysis is determined following Fernie (1989); Kato et al. (2010). We list the epoch of the superhump maxima in Table A4.

2.2 Archival time-domain surveys

We also extracted the all-sky photometric survey data from the All-Sky Automated Survey for SuperNovae (ASAS-SN) Sky Patrol (Shappee et al. 2014; Kochanek et al. 2017; Hart et al. 2023), the Asteroid Terrestrial-impact Last Alert System (ATLAS; Tonry et al. 2018; Heinze et al. 2018; Smith et al. 2020; Shingles et al. 2021), and the Catalina Surveys Data Release 3 (CRTS; Drake et al. 2009) to examine the global light curve profile in and before the outburst.

3 RESULTS

3.1 Overall light curve

The bottom panel of Figure 1 presents the global light curve of ASASSN-25dc around its 2025 outburst. The outburst rise was first detected by ATLAS in its o band on BJD 2460860.6 at $o \approx 17.2$ mag (top panel of Figure 2). The light curve showed a slow rise to the maximum on BJD 2460869.5 at $o \approx 13.4$ mag. A linear interpolation using the ATLAS o -band data between BJD 2460860–2460868 yields its rise timescale as $1.62(9)$ d mag $^{-1}$. Even with the data BJD 2460864–2460868, the rise timescale is $1.5(2)$ d mag $^{-1}$. The first outburst plateau on BJD 2460869.5–2460872.0 is characterised by a flat-top and symmetric profile rather than a powerlaw outburst decline typically observed in WZ Sge-type DNe with the 2:1 tidal resonance.

After the first outburst plateau, ASASSN-25dc showed a V-shaped 1.0-mag dip for ≈ 3.0 d on BJD 2460872.5–2460875.5 (bottom panel of Figure 2). After recovering from the dip, the second outburst plateau reached $c \approx 13.3$ mag on BJD 2460876.5. The decline rate on the second plateau was $35.2(1)$ d mag $^{-1}$ via a linear interpolation. The rapid decline from the outburst was observed on BJD 2460900.2. Thus, the duration of the second plateau is ≈ 25.0 d. The total duration of the outburst from its outburst rise is ≈ 40 d, including the dip. These numbers are comparable to those of other WZ Sge-type DNe (e.g., see Figure 11 of Tampo et al. 2024). After the rapid decline, no rebrightening outbursts have been observed, although a short rebrightening less than a day cannot be fully excluded due to the observation gaps.

ATLAS and ASASSN have observed ASASSN-25dc before this 2025 outburst since BJD 2457405 and 2456792, respectively. ATLAS provides continuous detections or upper limits around the quiescence level. Although ASASSN reports some sparse detections, these points cannot be considered as real events because there are upper limits or detections at the quiescence level within the same or a few nights by ASASSN or ATLAS. CRTS has 72 detections of the nearby star, Gaia object 6129070304518741376 ($G=18.678(3)$ mag, $4.3''$ from ASASSN-25dc), between BJD 2453589–2456047, while ASASSN-25dc has not been detected in this period, consistent with its quiescence level. Although we cannot exclude the possibility that

ASASSN-25dc had an outburst in the observation gap of CRTS and ASASSN, we conclude that there was no outburst of ASASSN-25dc at least in the past ≈ 10 years, and presumably in the past ≈ 20 years.

3.2 Superhumps and binary parameters

The single-peaked ordinary superhumps are clearly present in the light curve during the second outburst plateau. Based on the $O - C$ diagram (the upper panel of Figure 1), we determined the stage-A and stage-B superhump phases as BJD 2460873.3–2460881.6 and 2460882.5–2460899.5, respectively. The PDM analysis yields their superhump periods as $0.059387(5)$ and $0.058864(3)$ d, respectively (Figure 3). The period decrease from stage-A to stage-B superhumps is $0.88(1)\%$. The mean superhump amplitudes of stage-A and stage-B superhumps are 0.075 and 0.045 mag, respectively, and amplitudes of individual superhumps remain smaller than ≈ 0.1 mag throughout the outburst (the middle panel of Figure 1). The P_{dot} during the stage-B superhumps was measured as $-1.4(2) \times 10^{-5}$ cycle $^{-1}$. As the system enters the rapid decline from the outburst, superhumps shifted to post-superoutburst superhumps with a longer period, judging from the $O - C$ diagram, although PDM analysis did not show any significant periodicity due to the low signal-to-noise ratio of the data.

Judging in the $O - C$ diagram, the first identified peak of stage-A superhumps is on BJD 2460873.27 or $E = 18$ before the bottom of the dip (bottom panel of Figure 2). Some modulations are presented before this epoch. However, their peaks do not agree with the extrapolation from the maxima of stage-A superhumps. Additionally, we did not detect any periodicity around the superhump period before this epoch. Thus, we do not find any evidence of early superhumps in the first plateau, although our short (≈ 2 d) baseline of time-resolved observations before the dip does not allow us to completely exclude periodic variations before this epoch.

Because we did not detect any periods associated with the orbital period, we cannot use the relations between the mass ratio and the superhump period excess. However, Equation 30 in Kato (2022), which formulates the empirical relation between the P_{dot} during stage-B superhumps and mass ratio, can still be applied to ASASSN-25dc. Our P_{dot} indicates its mass ratio as $0.054(7)$. We stress that, WZ Sge-type DNe with similar superhump periods but above the period minimum ($q \approx 0.1$) show positive P_{dot} of $\sim 10 \times 10^{-5}$ cycle $^{-1}$ (Kato 2022), well larger than that of ASASSN-25dc. Given this mass ratio, the expected fractional excess ϵ^* ($= 1 - P_{\text{orb}}/P_{\text{SH}}$) of the stage-A superhump period is $0.020(3)$ (Table 1 in Kato 2022), indicating its orbital period as $0.0580(3)$ d. We note that future observations to determine its orbital period are still vital to confirm these binary parameters, including the mass ratio.

4 DISCUSSION

4.1 ASASSN-25dc as a period bouncer candidate

Our empirical orbital period and mass ratio of ASASSN-25dc indicate that ASASSN-25dc is located around the period minimum, and is even a candidate period bouncer (Figure 4). Other outburst characteristics of ASASSN-25dc also agree with those observed in some period bouncers and candidates (Kimura et al. 2018): the long duration of stage-A superhumps (≈ 150 cycles), small superhump amplitude (≈ 0.08 mag), a long decline timescale of the outburst plateau ($35.2(1)$ d mag $^{-1}$), and a large outburst amplitude at the time of emergence of ordinary superhumps (7.7 mag after the dip). On the other hand, ASASSN-25dc does not exhibit a large decrease

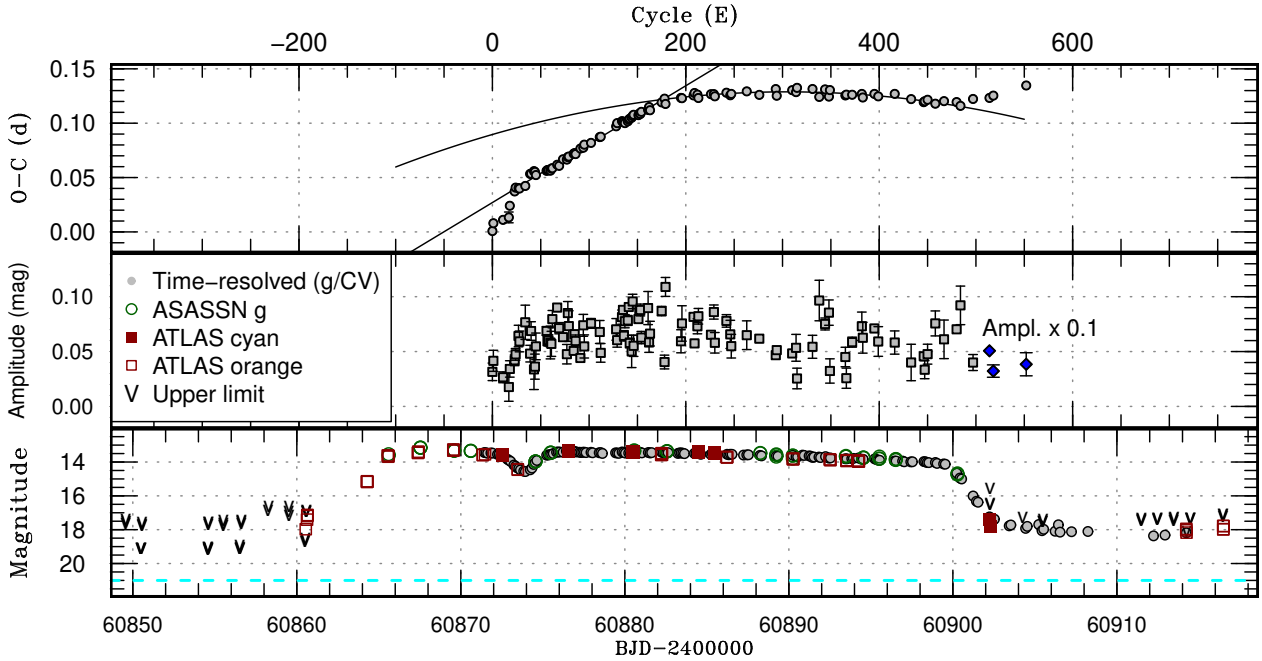


Figure 1. Top panel; $O - C$ diagram of superhump maxima. $C = \text{BJD } 2460871.87867 + 0.05885E$. The solid straight lines correspond to the periods of the stage-A superhumps. The curved line indicates the parabolic fit to the $O - C$ during the stage-B superhumps. Middle panel; Amplitude of superhumps in magnitude scale. The amplitudes after the rapid decline (after BJD 2460902.2; blue diamonds) are multiplied by 0.1 for visualisation purposes. Bottom panel; Overall optical light curve in outburst. The grey dots represent the data from VSNET and SAAO, binned in 0.1 d. The open circles, filled squares, and open squares represent the data of ASASSN g band, ATLAS c band, and ATLAS o band, respectively. The V-shaped markers indicate the upper limits. The horizontal dashed line represents the brightness of the counterpart in the Gaia EDR3 ($G=21.00(2)$ mag).

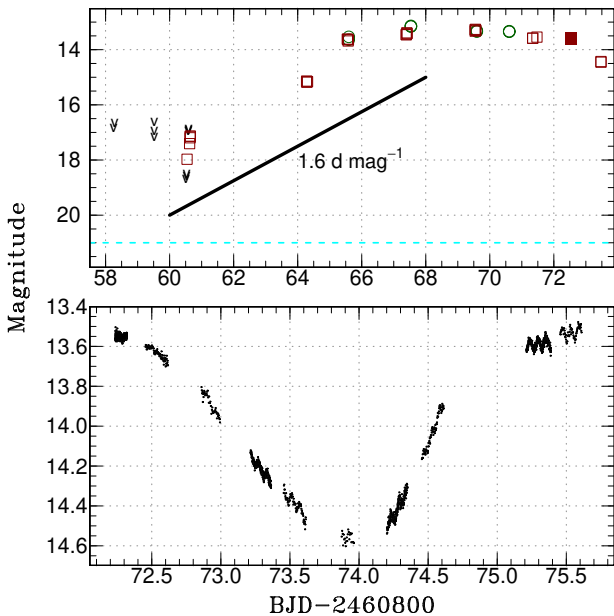


Figure 2. Zoomed light curves around the outburst rise (top) and the dip (bottom). Symbols are the same as Figure 1. The typical errors are smaller than the marker size. The solid line in the top panel represents the rise timescale of 1.6 d mag^{-1} .

between the stage-A and stage-B superhump periods. However, this may not be so critical, because the confirmed period bouncer SSS J122221.7–311523 and the suggested one ASASSN-16dt also show a small period decrease of an order of $\leq 1\%$ (Kimura et al. 2018).

Despite its short superhump period and proposed small mass ratio, we did not detect early superhumps in ASASSN-25dc. Although the amplitude of early superhumps and hence its detectability depend on the inclination of a system, a faster powerlaw decline in the early superhump phase is universally observed, including a low-inclination system (Kato 2015) and a system with the double-superoutburst property (Nakata et al. 2014; Kimura et al. 2018). This clearly differs from the flat-top profile of the first outburst plateau in ASASSN-25dc. A similar flat-top profile of the first outburst plateau was observed in SSS J122221.7–311523 (Kato et al. 2013). This system also showed a long stage-A superhump phase (≈ 200 cycles) and slow decline rate ($\approx 50 \text{ d mag}^{-1}$), although it has the even longer orbital period (0.07625(5) d) and lower mass ratio (0.032(2)) compared to ASASSN-25dc (Kato et al. 2013; Neustroev et al. 2017; Kimura et al. 2018). We here conclude that the 2:1 resonance indeed was not excited in ASASSN-25dc, rather than early superhumps were missed due to an observational bias of either a lower inclination or a short baseline of our time-resolved observations.

4.2 A slow-rise outburst in ASASSN-25dc

One of the significant differences of ASASSN-25dc from WZ Sge-type DNe is its long rise timescale. Table 1 compares the rise timescales of ASASSN-25dc and other WZ Sge-type DNe. It must be noted that the samples in Otulakowska-Hypka et al. (2016) should be treated as an upper limit, as their rise timescales are determined

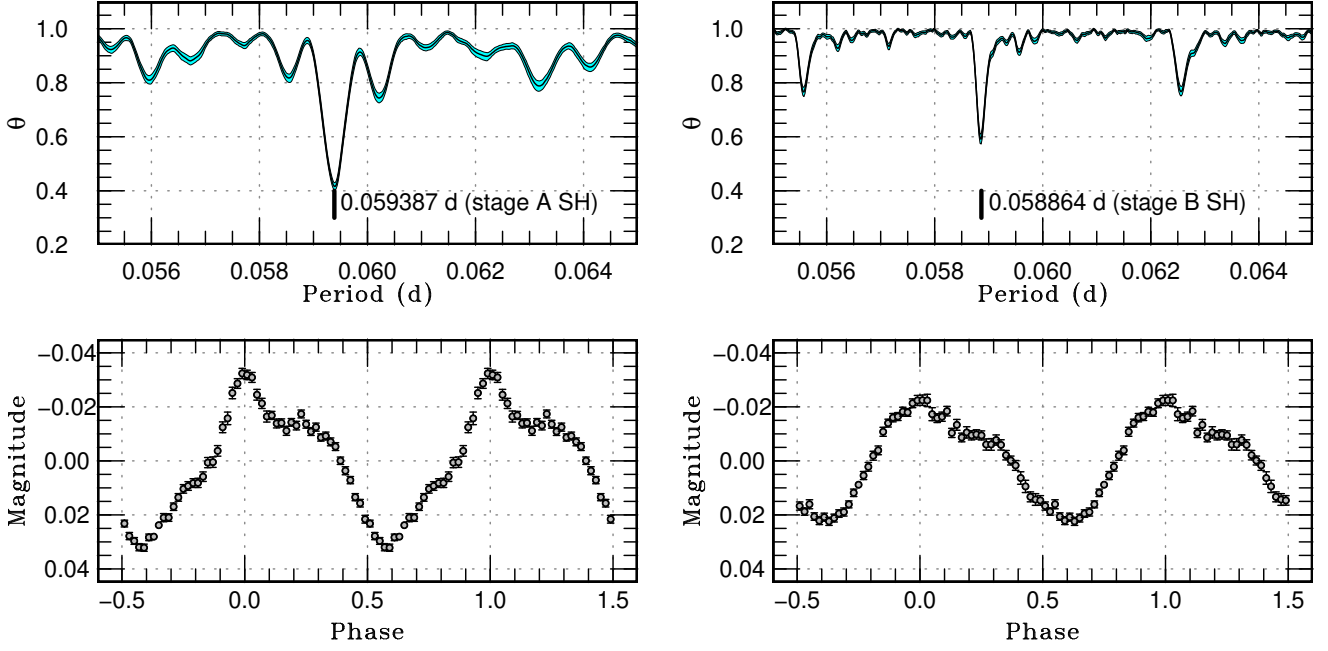


Figure 3. Results of PDM analysis (top) and phase-folded profiles (bottom) of stage-A (left) and stage-B (right) superhumps. The superhump phase is arbitrary. The obtained periods are $0.059387(5)$ and $0.058864(3)$ d, respectively.

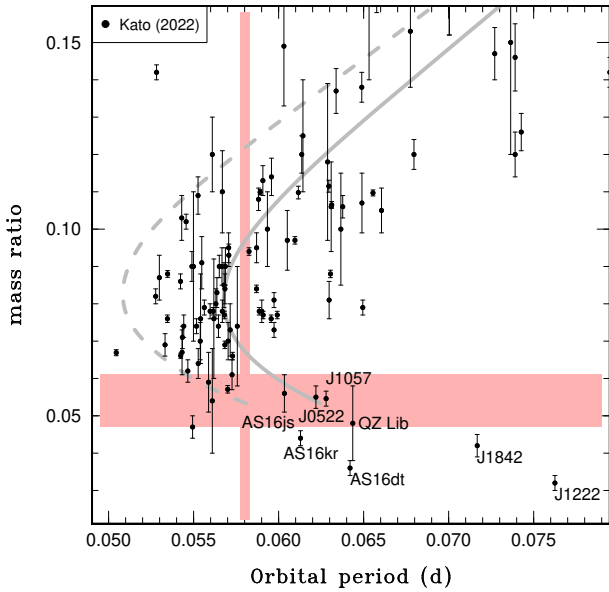


Figure 4. Orbital periods versus mass ratios of CVs around the period minimum. The shaded region indicates the possible ranges of those of ASASSN-25dc. Black points represent the samples in Kato (2022). The solid and dashed lines represent the standard and optimal evolutionary path of CVs in Knigge et al. (2011). Some notable systems beyond the period minimum ($P_{\text{orb}} > 0.06$ d and $q < 0.06$) are labelled with text. Their abbreviations are as follows; AS16dt = ASASSN-16dt, AS16js = ASASSN-16js, AS16kr = ASASSN-16kr, J0522 = CRTS J052209.7–350530, J1057 = SDSS J105754.25+275947.5, J1222 = SSS J122221.7–311523, J1842 = PNV J18422792+4837425 = V529 Dra.

solely by CRTS with 1-d cadence. This clearly demonstrates that the observed rise timescale in ASASSN-25dc is unambiguously longer than those less than 0.4 d mag^{-1} in WZ Sge-type DNe. In the case of SS Cyg, Cannizzo & Mattei (1998) showed that the rise timescale shows a bimodal distribution, of which the faster timescales are expressed as $0.56 \pm 0.14 \text{ d mag}^{-1}$ while the slower timescales exceed 1.0 d mag^{-1} . In Table 1, we also measure the rise timescales of outside-in and inside-out outbursts of an SU UMA-type DN V516 Lyr using Kepler data (Kato & Osaki 2013a, ; see also Appendix A). This also shows a similar distribution of rise timescales of outside-in and inside-out outbursts to those of SS Cyg. We note that the slightly longer rise timescales of outside-in outbursts in SS Cyg and V516 Lyr, than those of WZ Sge-type DNe, are likely due to their brighter quiescence. Thus, the observed rise timescale of ASASSN-25dc lies within the range of inside-out outbursts of SS Cyg and V516 Lyr, unlike other WZ Sge-type DNe.

4.3 Implications in the disc instability model

A dip in the outburst plateau separating the early and ordinary superhump phases has been regarded as a smoking-gun feature of period-bouncer systems (e.g. Kimura et al. 2018, and references therein). Their dip is understood as follows: The first superoutburst is maintained by the 2:1 resonance. Since the growth of the 3:1 resonance takes a longer time in a low-mass ratio system and is also suppressed by the 2:1 resonance (Lubow 1991a,b), the cooling wave started to propagate before the 3:1 tidal instability gets fully excited, which is observed as the growing ordinary superhumps in the dip. As the 3:1 resonance fully sets in, the disc returns to its outburst state, resulting in the typical behaviour of ordinary superhumps in the second superoutburst.

In the case of ASASSN-25dc, we consider that, without the excitement of the 2:1 resonance, the first outburst plateau is a precursor

Table 1. The outburst rise timescales of WZ Sge-type DNe and V516 Lyr

Name	τ_{rise} d mag ⁻¹	Reference*
ASASSN-25dc	1.62(9)	this work
ASASSN-23ba	0.208(3)	[1]
PNV J1903–31	0.169(1)	[1]
V748 Hya	0.066(1)	[1]
ASASSN-25ci	0.317(3)	[1]
V455 And	0.1	[2]
GW Lib	0.1	[3]
MASTER J0302+19	0.31(1)	[4]
AL Com	0.2	[5]
UZ Boo	0.3	[5]
V1108 Her	0.3	[5]
V516 Lyr (outside-in)	0.55(6)	[6]
V516 Lyr (inside-out)	1.15(7)	[6]

*[1]Tampo et al. (2026), [2]Maehara et al. (2009),
[3]Vican et al. (2011), [4]Tampo et al. (2024),
[5]Otulakowska-Hypka et al. (2016), [6]Kato & Osaki (2013a).

outburst powered by thermal instability and viscous depletion in a massive ($\approx 10^{24}$ g in a case of WZ Sge compared to $\approx 10^{23}$ g in standard SU UMa stars; Ichikawa et al. 1993; Smak 1993) disc (type B outburst in Osaki 2005), rather than a superoutburst powered by the 2:1 tidal resonance. A similar scenario is suggested in SSS J122221.7–311523 (Kato et al. 2013) and in EG Cnc (Kimura et al. 2021). This naturally explains the relatively short duration of the first outburst plateau compared to that of its second outburst plateau with ordinary superhumps. Once the 3:1 tidal resonance gets fully excited, the disc undergoes a superoutburst. Its just ≈ 4 -d delay of the emergence of ordinary superhumps from the outburst maximum, shorter than those of other low-mass ratio systems (Kimura et al. 2018), would be understood as the lack of the suppression of the 3:1 resonance by the 2:1 resonance, although it is unclear from the light curve exactly when the disc reached the 3:1 resonance radius.

The superoutburst of ASASSN-25dc is another example of a superoutburst from a low ($q \leq 0.1$) mass-ratio system, but lacking evidence of the excitation of the 2:1 tidal resonance. It has been found that some genuine WZ Sge-type DNe undergo a superoutburst lacking an early superhump phase, within a few years after the more energetic superoutburst with an early superhump phase. Kimura et al. (2016, 2021) discussed that an outburst somehow triggered in a less massive disc may explain this phenomenon. Such a scenario, however, cannot be applied to ASASSN-25dc, considering its long (≈ 40 d) outburst duration and no previous outbursts for at least the last 10 years before this 2025 superoutburst. Moreover, the 2022 superoutburst of the WZ Sge-type DN TCP J05515391+6504346, which lacked the early superhump phase, showed the rise timescale of 0.070(4) d mag⁻¹, within the range of other WZ Sge-type DNe with the early superhump phase (Tampo et al. 2026). Thus, a less massive disc does not necessarily lead to a longer rise timescale.

An alternative scenario we propose here is an inside-out superoutburst in the low-mass-ratio system ASASSN-25dc. The rise timescale of DN outbursts is regarded as a strong indication of whether an outburst is triggered as an outside-in or inside-out type outburst. Its long timescale within the range of inside-out outbursts of SS Cyg and V516 Lyr strongly supports this scenario. The symmetric profile of the first outburst plateau also agrees with this interpretation. Smak (1984); Mineshige & Osaki (1985) show that indeed a disc remains smaller in inside-out outbursts than in outside-in outbursts. This effect potentially prevents its disc from reaching the 2:1 resonance

radius and exciting the tidal instability in the first outburst plateau, even with its mass ratio low enough to excite the 2:1 tidal resonance.

This scenario, an inside-out outburst in a system around the period minimum, challenges the existing models explaining outbursts in WZ Sge-type DNe. Outbursts with a slow rise, suggesting an inside-out outburst, have been observed in a wide range of orbital periods from standard SU UMa-type DNe (e.g., Kato & Osaki 2013a; Sklyanov et al. 2018) to long-orbital-period DNe (Kim et al. 1992). However, various authors have found that simply lowering the mass transfer rate in a model for standard SU UMa-type DNe results in inside-out outbursts but with much less accreted mass (Smak 1993; Lasota et al. 1995; Osaki 1995), inconsistent with the long outburst duration of ASASSN-25dc and other WZ Sge-type DNe. To take into account the outburst energetics of WZ Sge-type DNe, two models have been mainly proposed: an inner disc truncation or an extremely low quiescence viscosity. In the case of an inner disc truncation and moderate quiescence viscosity ($\alpha_c \approx 0.01$), Lasota et al. (1995); Hameury et al. (1997) have suggested that an outburst must be triggered and maintained by the enhanced mass transfer from the secondary star since the disc mass before the outburst is much less than the critical surface density. This must always result in an outside-in outburst regardless of the state of the disc before the outburst. The simulated light curve in Hameury et al. (1997) indeed shows a rapid rise to the outburst maximum, unlike that of ASASSN-25dc. Osaki (1995); Meyer-Hofmeister et al. (1998) have found that a model with an extremely low quiescence viscosity ($\alpha_c \leq 0.001$) still requires a massive and large disc at the onset of an outburst, as the critical surface density is larger in the outer disc. The simulated light curve in Osaki (1995) also shows a rapid rise to the outburst maximum. One possible solution for altering this to an inside-out outburst is radial-dependent viscosity in quiescence. Larger viscosity α in an inner disc allows a shorter viscosity drift timescale and more mass in the inner disc. Some simulation studies found its radial dependence to be $\alpha \propto r^{0.5}$ (Mineshige & Wood 1989; Cannizzo 1993). Although a flatter radial dependence in the quiescent viscosity compared to other WZ Sge-type DNe may enable a massive disc to trigger an inside-out outburst, this still must require a rather different disc and system structure from other systems. Future observations, speculatively in the respects of the WD magnetosphere or the evaporation effect in the inner disc, and numerical simulations, to find a possible range for inner disc truncation and radial dependence of viscosity that can reproduce the light curve of ASASSN-25dc, are necessary to distinguish these scenarios.

5 SUMMARY

We have reported the optical time-resolved observations of a new dwarf nova system, ASASSN-25dc, during its 2025 superoutburst. We find superhumps in the outburst plateau with the periods of 0.059387(5) and 0.058864(3) d for stage-A and stage-B ordinary superhumps, respectively. The negative P_{dot} in stage-B superhumps ($-1.4(2) \times 10^{-5}$ cycle⁻¹) indicates its mass ratio as 0.054(7). The slow decline rate of the ordinary superhump phase and small superhump amplitude also support that ASASSN-25dc is a CV system around or even after the period bounce. The flat-top and symmetric profile of the first outburst plateau proposes that the 2:1 tidal resonance was not excited. Furthermore, its initial outburst rise is characterised by a rise timescale of 1.62(9) d mag⁻¹, significantly longer than those of other well-studied WZ Sge-type DNe. This suggests that the 2025 superoutburst of ASASSN-25dc was initially triggered as an inside-out outburst. These points illustrate a scenario in which

ASASSN-25dc is the first low-mass-ratio system with an inside-out dwarf nova superoutburst. This fact itself challenges the existing disc instability models explaining outbursts in WZ Sge-type DNe. An inner disc truncation model with an outburst triggered by the enhanced mass transfer cannot reproduce an inside-out outburst. A significant modification, especially in the disc and system structure in quiescence, is still necessary to explain all the observed phenomena in the framework of the thermal-tidal instability model with very low viscosity.

ACKNOWLEDGEMENTS

We acknowledge amateur and professional astronomers around the world who have shared data on variable stars and transients with the VSNET collaboration. This paper uses observations made from the South African Astronomical Observatory (SAAO). This work has made use of data from the Asteroid Terrestrial-impact Last Alert System (ATLAS) project. The Asteroid Terrestrial-impact Last Alert System (ATLAS) project is primarily funded to search for near earth asteroids through NASA grants NN12AR55G, 80NSSC18K0284, and 80NSSC18K1575; byproducts of the NEO search include images and catalogs from the survey area. The ATLAS science products have been made possible through the contributions of the University of Hawaii Institute for Astronomy, the Queen's University Belfast, the Space Telescope Science Institute, the South African Astronomical Observatory, and The Millennium Institute of Astrophysics (MAS), Chile.

DATA AVAILABILITY

Most of the ground-based observations are publicly available at the American Association of Variable Star Observers (AAVSO) International Database (<https://www.aavso.org/>). Other data is available upon request to individual observers.

REFERENCES

- Cannizzo J. K., 1993, *ApJ*, 419, 318
 Cannizzo J. K., 2001, *ApJ*, 561, L175
 Cannizzo J. K., Mattei J. A., 1998, *ApJ*, 505, 344
 Cannizzo J. K., Shafter A. W., Wheeler J. C., 1988, *ApJ*, 333, 227
 Cleveland W. S., 1979, *J. Amer. Statist. Assoc.*, 74, 829
 Coppejans R., et al., 2013, *PASP*, 125, 976
 Drake A. J., et al., 2009, *ApJ*, 696, 870
 Erasmus N., et al., 2024, *Journal of Astronomical Telescopes, Instruments, and Systems*, 10, 025005
 Fernie J. D., 1989, *PASP*, 101, 225
 Gaia Collaboration et al., 2021, *A&A*, 649, A1
 Gänsicke B. T., et al., 2009, *MNRAS*, 397, 2170
 Hameury J. M., 2020, *Advances in Space Research*, 66, 1004
 Hameury J.-M., Lasota J.-P., Hure J.-M., 1997, *MNRAS*, 287, 937
 Hart K., et al., 2023, preprint, (arXiv:2304.03791)
 Heinze A. N., et al., 2018, *AJ*, 156, 241
 Hellier C., 2001, *Cataclysmic Variable Stars*. Berlin: Springer
 Hirose M., Osaki Y., 1990, *PASJ*, 42, 135
 Ichikawa S., Hirose M., Osaki Y., 1993, *PASJ*, 45, 243
 Kato T., 2015, *PASJ*, 67, 108
 Kato T., 2022, *VSOLJ Variable Star Bull.*, 89, arXiv:2201.02945
 Kato T., Osaki Y., 2013a, *PASJ*, 65, 97
 Kato T., Osaki Y., 2013b, *PASJ*, 65, 115
 Kato T., Uemura M., Ishioka R., Nogami D., Kunjaya C., Baba H., Yamaoka H., 2004, *PASJ*, 56, S1
 Kato T., et al., 2009, *PASJ*, 61, S395
 Kato T., et al., 2010, *PASJ*, 62, 1525
 Kato T., Monard B., Hamsch F.-J., Kiyota S., Maehara H., 2013, *PASJ*, 65, L11
 Kim S.-W., Wheeler J. C., Mineshige S., 1992, *ApJ*, 384, 269
 Kimura M., 2020, *Observational and Theoretical Studies on Dwarf-nova Outbursts*, 1 edn. Springer Theses, Springer Singapore, doi:10.1007/978-981-15-8912-6
 Kimura M., et al., 2016, *PASJ*, 68, L2
 Kimura M., et al., 2018, *PASJ*, 70, 47
 Kimura M., et al., 2021, *PASJ*, 73, 1
 King A. R., 1988, *QJRAS*, 29, 1
 Knigge C., Baraffe I., Patterson J., 2011, *ApJS*, 194, 28
 Kochanek C. S., et al., 2017, *PASP*, 129, 104502
 Lasota J. P., Hameury J. M., Hure J. M., 1995, *A&A*, 302, L29
 Lin D. N. C., Papaloizou J., 1979, *MNRAS*, 186, 799
 Lubow S. H., 1991a, *ApJ*, 381, 259
 Lubow S. H., 1991b, *ApJ*, 381, 268
 Maehara H., et al., 2009, in S. J. Murphy & M. S. Bessell ed., *ASP Conf. Ser. 404, The Eighth Pacific Rim Conference on Stellar Astrophysics: A Tribute to Kam-Ching Leung*. San Francisco: ASP, pp 57–63
 McAllister M., et al., 2019, *MNRAS*, 486, 5535
 Meyer-Hofmeister E., Meyer F., Liu B. F., 1998, *A&A*, 339, 507
 Mineshige S., Osaki Y., 1985, *PASJ*, 37, 1
 Mineshige S., Wood J. H., 1989, *MNRAS*, 241, 259
 Nakata C., et al., 2014, *PASJ*, 66, 116
 Neustroev V. V., et al., 2017, *MNRAS*, 467, 597
 Osaki Y., 1995, *PASJ*, 47, 47
 Osaki Y., 1996, *PASP*, 108, 39
 Osaki Y., 2005, *Proceedings of the Japan Academy, Series B*, 81, 291
 Osaki Y., Meyer F., 2002, *A&A*, 383, 574
 Otulakowska-Hypka M., Olech A., Patterson J., 2016, *MNRAS*, 460, 2526
 Patterson J., McGraw J. T., Coleman L., Africano J. L., 1981, *ApJ*, 248, 1067
 Patterson J., et al., 2005, *PASP*, 117, 1204
 Robinson E. L., 1983, in Livio M., Shaviv G., eds, *Astrophysics and Space Science Library Vol. 101, IAU Colloq. 72: Cataclysmic Variables and Related Objects*. Springer Nature, pp 1–14, doi:10.1007/978-94-009-7118-9_1
 Shappee B. J., et al., 2014, *ApJ*, 788, 48
 Shingles L., et al., 2021, *Transient Name Server AstroNote*, 7, 1
 Sklyanov A. S., et al., 2018, *Astrophysics*, 61, 64
 Smak J., 1984, *PASP*, 96, 5
 Smak J., 1993, *Acta Astron.*, 43, 101
 Smith K. W., et al., 2020, *PASP*, 132, 085002
 Stellingwerf R. F., 1978, *ApJ*, 224, 953
 Tampo Y., et al., 2024, *PASJ*, 76, 1228
 Tampo Y., et al., 2026, *MNRAS*, 545, staf1964
 Tonry J. L., et al., 2018, *PASP*, 130, 064505
 Uemura M., Kato T., Ohshima T., Maehara H., 2012, *PASJ*, 64, 92
 Vican L., et al., 2011, *PASP*, 123, 1156
 Warner B., 1995, *Cataclysmic variable stars*. Cambridge: Cambridge University Press
 Whitehurst R., 1988, *MNRAS*, 232, 35

APPENDIX A: RISE TIMESCALES OF V516 LYR

Although the rise timescale measurements of SS Cyg in Cannizzo & Mattei (1998) provide a meaningful sample, SS Cyg is much brighter in quiescence, and its disc is larger than CVs around the period minimum, which apparently affects the rise timescale. Moreover, they claim that their sample of SS Cyg still may suffer from the 1-d aliases. To reliably measure the rise timescales of inside-out outbursts in a system with a short orbital period (i.e., below the period gap), we utilized the light curve of V516 Lyr ($P_{\text{orb}} = 0.083999(8)$ d) observed by Kepler with a 30-min cadence. We used only the outbursts confidently labelled as either a normal outside-in or inside-out outbursts in Kato & Osaki (2013a). To qualitatively measure the rise timescale, we first obtained the smoothed light curve by LOWESS and determined the epoch of the outburst maximum (Figure A1). We then fitted the light curve in the magnitude scale with a broken linear function ($F(t)$; Equation A1) using the data between 0.2–2.5 days before the outburst maximum, covering both the quiescence and outburst rise,

$$F(t) = \begin{cases} c, & t \leq t_{\text{outburst}} \\ c - \frac{1}{\tau_{\text{rise}}} (t - t_{\text{outburst}}), & t > t_{\text{outburst}} \end{cases} \quad (\text{A1})$$

where t_{outburst} , τ_{rise} , and c are the epoch when the outburst starts, the rise timescale, and the constant brightness in quiescence.

Table A1 lists the measured rise timescales of 21 outbursts, in the unit of d mag^{-1} , 12 of which are outside-in outbursts, and the remaining 9 are inside-out outbursts. Among the outbursts listed as outside-in, Q10-3, Q10-9, and Q14-7 show a shoulder on the outburst rise, which prolongs the measured rise timescales. Although Q9-1 and Q9-4 are classified as inside-out outbursts, they show short rise timescales comparable to those of outside-in outbursts. Indeed, their outburst profile resembles some of the outside-in outbursts. As Kato & Osaki (2013a) claimed, since their outburst type is flagged by eye, we excluded these five outbursts, and measured the median rise timescales of 9 outside-in and 7 inside-out outbursts as the confident sample, which are listed in Table 1.

APPENDIX B: OBSERVATION LOGS

This paper has been typeset from a \LaTeX file prepared by the author.

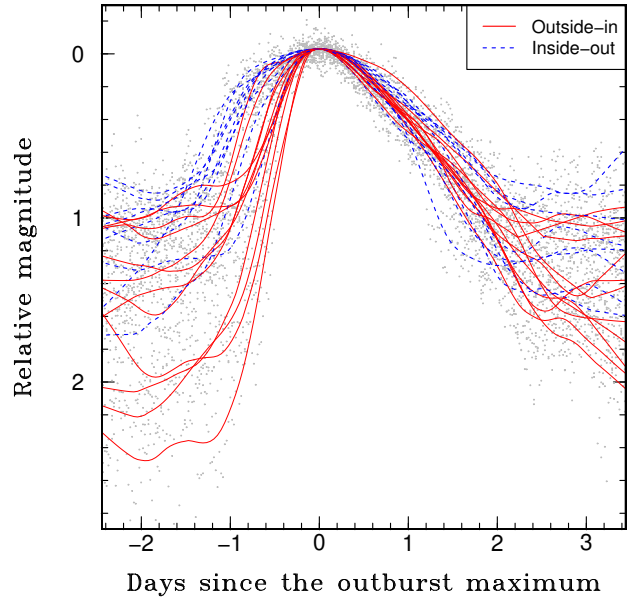


Figure A1. The outburst light curves of V516 Lyr observed by Kepler (gray circles). They are normalized at the outburst maximum and its epoch. The blue-dashed and red-solid lines represent the smoothed ones of inside-out and outside-in outbursts.

Table A1. Rise timescales of V516 Lyr observed by Kepler

Outburst*	Type	τ_{rise} d mag^{-1}	Error d mag^{-1}
Q6-4	outside-in	0.38	0.03
Q6-5	outside-in	0.29	0.02
Q7-1	outside-in	0.66	0.06
Q7-3	outside-in	0.29	0.02
Q7-4	outside-in	0.45	0.03
Q8-4	outside-in	0.37	0.03
Q9-1	inside-out	0.44	0.02
Q9-3	inside-out	1.12	0.03
Q9-4	inside-out	0.67	0.03
Q9-5	outside-in	0.88	0.10
Q9-7	inside-out	1.03	0.06
Q10-2	inside-out	1.08	0.07
Q10-3 [†]	outside-in	0.76	0.05
Q10-7	outside-in	0.54	0.06
Q10-8	outside-in	0.55	0.03
Q10-9 [†]	outside-in	0.77	0.05
Q14-1	inside-out	1.15	0.05
Q14-2	inside-out	1.35	0.06
Q14-3	inside-out	1.49	0.10
Q14-6	inside-out	1.22	0.06
Q14-7 [†]	outside-in	0.73	0.03

*Outburst ID in Kato & Osaki (2013a).

[†]Outburst with a shoulder rise.

Table A2. List of instruments for photometric observation

Observer's code	Telescope(& CCD)	Observatory (or Observer)
GPX	25cm reflector+ZWO ASI178mm	W. Goltz
HaC	35cm C14+QHY600M	F. J. Hambusch
LSD	1.0m Lesedi+Mookodi	SAAO
MLF	30cm RCX400+ST8-XME	B. Monard
S40	1.0m+SHOC	SAAO
SPE	30cm RCX400+ST8-XME	P. Starr

Table A3. Log of ground-based time-resolved photometric observations

Start*	End*	Mag [†]	$\sigma_{\text{Mag}}^{\ddagger}$	N^{\S}	Obs	Band	Start*	End*	Mag [†]	$\sigma_{\text{Mag}}^{\ddagger}$	N^{\S}	Obs	Band
871.4547	871.6204	13.458	0.002	93	HaC	CV	888.2090	888.2952	13.358	0.001	411	LSD	g
871.8624	871.9826	13.417	0.002	50	GPX	CV	889.2095	889.3050	13.390	0.001	468	LSD	g
872.2368	872.3203	13.418	0.000	660	LSD	g	889.2122	889.3567	13.427	0.001	291	MLF	CV
872.4545	872.6173	13.635	0.003	97	HaC	CV	890.2185	890.2595	13.437	0.001	230	LSD	g
872.8595	872.9936	13.836	0.007	52	GPX	CV	890.4579	890.5668	13.689	0.003	66	HaC	CV
873.2150	873.3630	14.001	0.002	295	MLF	CV	890.8684	890.9369	13.690	0.006	28	GPX	CV
873.4546	873.6147	14.397	0.005	93	HaC	CV	891.2566	891.2976	13.486	0.001	230	LSD	g
873.8740	873.9627	14.505	0.005	25	GPX	CV	891.4585	891.5116	13.715	0.003	29	HaC	CV
874.2021	874.3497	14.200	0.003	289	MLF	CV	891.8834	891.9608	13.818	0.007	33	GPX	CV
874.4548	874.6122	14.023	0.009	93	HaC	CV	892.2249	892.2656	13.523	0.002	193	LSD	g
875.2111	875.3886	13.374	0.001	355	MLF	CV	892.4584	892.5616	13.760	0.003	65	HaC	CV
875.4555	875.6098	13.529	0.003	79	HaC	CV	893.4584	893.5584	13.810	0.002	57	HaC	CV
875.8575	876.0388	13.562	0.002	200	SPE	CV	893.8649	893.9446	13.967	0.002	100	SPE	CV
876.1947	876.2813	13.369	0.001	1475	S40	g	894.2093	894.2501	13.605	0.001	229	LSD	g
876.4557	876.6063	13.371	0.003	69	HaC	CV	894.4585	894.5561	13.839	0.003	51	HaC	CV
876.8560	877.0402	13.535	0.002	214	SPE	CV	895.2346	895.2932	13.660	0.001	329	LSD	g
877.2573	877.3332	13.678	0.001	1172	S40	CV	895.4590	895.5538	13.895	0.003	53	HaC	CV
877.4553	877.6043	13.423	0.003	68	HaC	CV	896.4592	896.5495	13.940	0.003	46	HaC	CV
877.9259	878.0296	13.590	0.002	131	SPE	CV	896.9560	897.0374	14.151	0.003	103	SPE	CV
878.4554	878.6005	13.452	0.003	71	HaC	CV	897.4593	897.5477	13.986	0.003	46	HaC	CV
879.4560	879.5969	13.466	0.003	65	HaC	CV	898.2200	898.3487	13.805	0.002	255	MLF	CV
879.8565	880.0783	13.617	0.002	279	SPE	CV	898.2248	898.2835	13.815	0.001	328	LSD	g
880.2102	880.3583	13.246	0.002	286	MLF	CV	898.4592	898.5452	14.034	0.002	44	HaC	CV
880.2241	880.3217	13.220	0.001	335	LSD	g	898.9403	899.0234	14.233	0.003	105	SPE	CV
880.4561	880.5953	13.445	0.004	64	HaC	CV	899.4640	899.5415	14.127	0.004	43	HaC	CV
880.8546	881.0584	13.605	0.002	255	SPE	CV	900.2131	900.2802	14.493	0.001	335	LSD	g
881.4561	881.5926	13.459	0.003	108	HaC	CV	900.4596	900.5398	14.989	0.006	45	HaC	CV
882.2669	882.3307	13.195	0.001	340	LSD	g	901.2130	901.2806	15.849	0.002	337	LSD	g
882.4562	882.5900	13.462	0.003	111	HaC	CV	901.4597	901.5365	16.365	0.010	41	HaC	CV
883.2578	883.2988	13.227	0.002	230	LSD	g	902.2115	902.2702	17.720	0.009	321	LSD	g
883.4562	883.5869	13.474	0.004	73	HaC	CV	902.4596	902.5343	17.417	0.019	51	HaC	CV
884.2104	884.3361	13.278	0.002	252	MLF	CV	903.4599	903.5297	17.740	0.022	37	HaC	CV
884.2359	884.3226	13.236	0.001	460	LSD	g	904.4601	904.5283	17.850	0.024	37	HaC	CV
884.4568	884.5839	13.503	0.003	134	HaC	CV	905.2146	905.2150	18.161	0.049	3	LSD	g
885.2755	885.3142	13.272	0.002	217	LSD	g	905.4601	905.5248	18.005	0.027	38	HaC	CV
885.4568	885.5810	13.520	0.003	107	HaC	CV	906.2297	906.2302	18.568	0.124	3	LSD	g
886.2293	886.2964	13.296	0.001	323	LSD	g	906.4605	906.5229	18.029	0.049	35	HaC	CV
886.4574	886.5782	13.545	0.003	69	HaC	CV	907.2526	907.2530	18.588	0.055	3	LSD	g
887.2313	887.2340	13.336	0.002	16	LSD	g	908.2207	908.2211	18.573	0.061	3	LSD	g
887.4575	887.5761	13.572	0.005	71	HaC	CV	912.2438	912.2443	18.835	0.086	3	LSD	g

*BJD-2460000

[†]Mean magnitude.

[‡]Standard deviation of the observed magnitude.

[§]Number of observations.

^{||}Observer's codes are same as table 1

Table A4. Times of superhump maxima

<i>E</i>	maximum time*	error	$O - C^\dagger$	N^\ddagger	<i>E</i>	maximum time*	error	$O - C^\dagger$	N^\ddagger
0	871.87943	0.00137	0.00076	18	154	881.05201	0.00082	0.11044	38
1	871.94550	0.00165	0.00798	19	161	881.46573	0.00063	0.11221	24
11	872.53709	0.00122	0.01107	24	162	881.52726	0.00099	0.11489	32
17	872.89245	0.00496	0.01333	18	163	881.58314	0.00153	0.11192	27
18	872.96201	0.00163	0.02404	19	175	882.29658	0.00018	0.11916	249
23	873.26943	0.00076	0.03721	93	178	882.47656	0.00103	0.12259	30
24	873.33181	0.00078	0.04074	94	179	882.53052	0.00058	0.11770	32
27	873.50795	0.00125	0.04033	24	195	883.47770	0.00127	0.12328	24
28	873.56635	0.00101	0.03988	24	196	883.53627	0.00151	0.12300	23
34	873.92186	0.00154	0.04229	13	208	884.24502	0.00016	0.12554	284
39	874.22718	0.00091	0.05336	89	209	884.30611	0.00026	0.12779	321
40	874.28617	0.00078	0.05350	93	212	884.48116	0.00066	0.12629	41
43	874.46514	0.00217	0.05592	18	213	884.53689	0.00052	0.12317	47
44	874.52324	0.00204	0.05517	24	226	885.30543	0.00028	0.12666	198
45	874.57921	0.00146	0.05229	26	229	885.48206	0.00054	0.12674	39
56	875.23046	0.00034	0.05619	95	230	885.53889	0.00094	0.12472	37
57	875.29009	0.00050	0.05697	95	242	886.24842	0.00047	0.12805	203
58	875.34864	0.00066	0.05668	93	246	886.48146	0.00112	0.12569	23
60	875.46600	0.00110	0.05633	17	247	886.54157	0.00116	0.12695	28
61	875.52677	0.00149	0.05825	20	263	887.48551	0.00187	0.12929	23
62	875.58595	0.00065	0.05858	23	276	888.24735	0.00026	0.12608	236
67	875.88340	0.00024	0.06178	59	293	889.25313	0.00032	0.13141	331
69	876.00008	0.00055	0.06076	59	294	889.30584	0.00050	0.12527	220
73	876.24152	0.00021	0.06680	792	310	890.25255	0.00039	0.13038	164
77	876.47664	0.00109	0.06652	21	314	890.48615	0.00132	0.12858	23
78	876.53781	0.00083	0.06884	20	315	890.54896	0.00281	0.13254	28
79	876.59718	0.00172	0.06936	17	331	891.48948	0.00145	0.13146	22
84	876.89396	0.00048	0.07189	59	338	891.89414	0.00085	0.12417	16
85	876.95344	0.00043	0.07252	42	344	892.25418	0.00063	0.13111	173
86	877.01135	0.00054	0.07158	59	348	892.48294	0.00084	0.12447	22
91	877.31073	0.00048	0.07670	659	349	892.54779	0.00268	0.13047	24
94	877.48801	0.00103	0.07744	20	365	893.48443	0.00138	0.12551	20
95	877.54969	0.00153	0.08027	20	366	893.54403	0.00203	0.12626	18
102	877.96326	0.00043	0.08189	59	372	893.89704	0.00047	0.12616	59
111	878.49824	0.00107	0.08722	20	382	894.48629	0.00099	0.12692	20
112	878.55744	0.00131	0.08757	22	383	894.54186	0.00181	0.12364	21
128	879.50860	0.00102	0.09713	20	395	895.25137	0.00024	0.12695	216
129	879.57040	0.00079	0.10008	22	399	895.48451	0.00175	0.12470	20
134	879.86647	0.00030	0.10190	42	416	896.48726	0.00166	0.12698	20
135	879.92464	0.00026	0.10122	59	433	897.48289	0.00242	0.12217	21
136	879.98351	0.00051	0.10124	59	446	898.24512	0.00040	0.11935	340
137	880.04119	0.00047	0.10007	59	447	898.30482	0.00211	0.12020	105
140	880.21939	0.00026	0.10172	243	450	898.48273	0.00122	0.12156	21
141	880.27973	0.00031	0.10321	145	458	898.94992	0.00060	0.11795	45
142	880.33950	0.00064	0.10413	82	467	899.48192	0.00165	0.12030	19
144	880.45810	0.00169	0.10503	13	480	900.24611	0.00032	0.11944	264
145	880.51858	0.00044	0.10665	20	484	900.47802	0.00109	0.11595	20
146	880.57851	0.00131	0.10774	21	497	901.24942	0.00127	0.12230	262
151	880.87243	0.00026	0.10741	55	514	902.25082	0.00041	0.12325	234
152	880.93282	0.00028	0.10895	59	518	902.48836	0.00096	0.12539	30
153	880.99124	0.00040	0.10852	59	552	904.49857	0.00151	0.13470	22

*BJD-2460000

† $C = \text{BJD } 2460871.87867 + 0.05885 \times E$.

‡Number of points used to determine the maximum.